Chemokine Receptor Inhibitor vMIP-II Promoting Lymphocytes in COVID-19 Patients and Its Related Mechanism In Vitro

Shiyu Li
Jinan University
Yuzhe Wang
Jinan University
Lixia Feng
Nanyang People's Hospital
Zhenyou Jiang
Jinan University
Feng Cong
Guangdong Laboratory Animal Monitoring Institute
Youyu Chen
Jinan University
Zhenning Dai
Jinan University
Shuting Liu
Jinan University
Shitao Zhu
Institute of Respiratory Diseases
Zhengbin Fei
Jinan University
Yichao Xu
Southern Medical University
Xuemei Mo
Jinan University
Shanshan Shi
Jinan University
Xiao Zheng
Jinan University
Anding Xu (tlil@jnu.edu.cn)
Guangzhou Overseas Chinese Hospital
Yong Gao (docgao@163.com)

Union Hospital
Wenhua Huang (✉ huangwenhua2009@sina.com)
Southern Medical University
Nuofu Zhang (✉ nfzhanggird@163.com)
Institute of Respiratory Diseases
Hanxiao Sun (✉ sunhx718@163.com)
Jinan University

Research Article

Keywords: SARS-CoV-2, Immune exhaustion, cellular immune reconstitution factor, inhibtor for chemokine receptors, vMIP-II, effector CD8+ T cell differentiation, central memory CD8+T cells, stem proliferation of effector CD8+ T cells, metabolic modulation

Posted Date: May 28th, 2020

DOI: https://doi.org/10.21203/rs.3.rs-31620/v1

Abstract

Coronavirus disease (COVID-19) accompanies severe immune injury as well as a decrease and overactivation of T lymphocytes. We observed that vMIP-Ⅱ, a broad-spectrum chemokine receptor inhibitor, could improve the lymphocyte decrease of COVID-19. Comparisons of T cell populations in PBMCs showed that the effects of vMIP-II on the subsets of T cells and cytokine secretion stimulated by SARS-CoV-2 S protein were the same as those in the asymptomatic infection group: the proportion of $CD8^+T_{CM}$ cells in the vMIP-II treatment and asymptomatic groups was significantly higher than that in the symptomatic control group. Differential gene expression of effector $CD8^+$ T cells suggested that vMIP-II inhibits multiple chemokine receptors and related signal pathway and strengthens their stem proliferating capacity. Thus, vMIP-II reconstitutes cellular immunity lost due to acute infection of SARS-CoV-2 by modulating effector $CD8^+$ T cells to produce more T_{CM} cells.

Introduction

In December 2019, the epidemic scale of severe acute respiratory syndrome coronavirus 2 (SARS-CoV-2), which first appeared in Wuhan, China, increased rapidly[1]. At present, cases of coronavirus disease (COVID-19) caused by SARS-CoV-2 have been found in many countries around the world[2]. By April 30th, 2020, there were 3,151,252 confirmed cases and 229,122 deaths worldwide. SARS-CoV-2 can cause systemic infection or damage in a variety of animals. Human infections often cause severe clinical symptoms and high mortality[3]. Autopsy reports of COVID-19 cases have shown that the numbers of peripheral $CD4^+$ and $CD8^+$ T cells were dramatically reduced, but the cells were over-activated. Over-activation of T cells is characterized by an increase in Th17 and high cytotoxicity of $CD8^+$ T cells, which explains the severe immune injury seen in patients. That is, there is a significant depletion of $CD8^+$ T cells[4,5].

Viral macrophage inflammatory protein-Ⅱ (vMIP-Ⅱ) is a small-molecule protein with high homology to human chemokine hMIP-1α and is encoded by the K4 gene of Kaposi's sarcoma herpesvirus (KSHV). vMIP-II interacts with human chemokine receptors using its structural framework, which is similar to that of other chemokines. With its ability to bind multiple human chemokine receptor subfamilies, vMIP-II is widely recognized as a broad-spectrum chemokine receptor inhibitor. It has been proven that vMIP-II has antagonistic activity against CCR1, CCR2B, CCR5, CCR8, CXCR3, and CXCR4, but not against CXCR1 or CXCR2. Its effect on CCR7 has not been clearly reported[6-11]. We previously found that vMIP-II competitively inhibits the binding of HIV to the co-receptors CCR5, CXCR4, and CCR3, among others, and used vMIP-II to prevent the virus from entering target cells and to study its role in resisting HIV infection[12,13]. In vivo vMIP-II experiments have shown that vMIP-II alters the $CD8^+$ T cell expression of some TCRVβ subfamilies in cynomolgus monkeys in the early stages of SIV infection. After treatment with vMIP-II in cynomolgus monkey, the $CD8^+$ T cells of some Vβ subfamilies showed remarkable proliferation, and the pedigree of the proliferative TCRVβ subfamily changed, indicating that vMIP-II

promotes proliferation and expression of this Vβ subfamily of $CD8^+$ T cells, suggesting that vMIP-II enhances the response of the immune system and promotes proliferation of specific immune cells in SIV infection[14-16]. In fact, our research on recombinant vMIP-II using the above SIV cynomolgus monkey model and the treatment of human AIDS (data not yet published) has shown that vMIP-II significantly increases the specific cell immune response in infected organisms and has a effect of reducing plasma viral load on the viremia period. Considering the pathological damage caused by effector $CD8^+$ T cell overactivation in COVID-19, vMIP-II may have an ameliorating effect. This study examined the efficacy of vMIP-II in clinical patients with COVID-19.

The SARS-CoV-2 genome is + ssRNA with a total length of approximately 30 kb. The first 2/3 of the genome encodes replicase, and the last 1/3 mainly encodes 4 structural proteins, including a spike protein (S protein), envelope protein (E protein), membrane protein (M protein), and nuclear protein (N protein) from 5' to 3'. Of these structural proteins, S protein mediates the adhesion and entry of coronavirus to host cells by binding host cell surface proteins or carbohydrate receptors. Thus, S protein determines host tropism and has become the main target for the development of antiviral drugs. The receptor-binding domain contained in S protein is lowly conserved among different viruses and contains a majority of its conformational neutralizing epitopes, which allow the virus to easily spread across tissue types and even species barriers among a wide range of hosts[17]. The receptor-binding domain is also the main antigenic epitope used in vaccine preparation. Most previous vaccine research on SARS-CoV and MERS-CoV used viral vector vaccines containing full-length or partial fragments of S protein as antigens[18-20]. Therefore, current vaccine research and development related to SARS-CoV-2 also focuses on S protein. For example, the University of Queensland in Australia will use its unique "molecular clamp" vaccine platform to change SARS-CoV-2 S protein synthesized in vitro into a natural polymeric state to facilitate induction and production of neutralizing antibodies *in vivo*[21]. Beijing AidiWeixin Biology will cooperate with Inovio Company in the United States to develop a DNA vaccine, "INO-4800," containing the SARS-CoV-2 S protein sequence[21]. However, the immune mechanism stimulated by SARS-CoV-2 in the human body is not very clear, especially as it relates to the destruction of cellular immunity caused by the virus, which may also be the main pathological mechanism. Regardless, the antigenic activity of S protein needs to be further elucidated.

Generally, after viral infection, $CD8^+$ T cells undergo three processes: expansion, contraction, and memory formation. Activated $CD8^+$ T cells are classified into short-lived effector cells (SLECs, characterized as KLRG1hiCD127low) and memory precursor effector cells (MPECs, characterized as KLRG1lowCD127hi). SLECs can produce a large number of cytotoxic molecules and cytokines, most of which are apoptotic during the contraction phase, while MPECs cells further differentiate into memory cells[22]. Memory cells are divided into central memory T cells (T_{CM} cells, with the phenotype $CD45RA^-CD45RO^+CCR7^+CD62L^+$), effector memory T cells (T_{EM} cells, with the phenotype $CD45RA^-CD45RO^+CCR7^-CD62L^-$), and tissue resident memory T cells (T_{RM}, with the phenotype $CD103^+CD69^+CD62L^-CD27^-$)[23-25]. Under sustained stimulation by antigens, $CD8^+$ T cells were exhausted (exhausted T cells, or T_{EX} cells), showing low levels

of IL-2, TNF-α, and INF-γ and high levels of PD-1, TAG3, CD244, CD160, and other inhibitory molecules on the cell surface. Studies have shown that memory $CD8^+$ T cells are a subset of effector T cells, inhibiting the expression of naïve-related genes to reverse differentiation of effector $CD8^+$ T cells into long-lived memory $CD8^+$ T cells[26].

There is currently no specific drug for the prevention or treatment of SARS-CoV-2 infection. An important strategy used to solve the problems of fast replication, wide host range, high variation, and fast cross-species spread that characterize SARS-CoV-2 is the development of broad-spectrum antiviral drugs, including nucleic acid synthesis inhibitors, protease inhibitors, RNA polymerase inhibitors, membrane fusion inhibitors, compound inhibitors, and even new applications of existing drugs[27,28]. Considering the immune damage and immune failure caused by SARS-CoV-2 infection, drugs that promote immune reconstitution will undoubtedly emerge as an important new research focus.

To further elucidate the role of vMIP-II in T cell immune remodeling after SARS-CoV-2 infection, we studied the differentiation mechanism of $CD8^+$ T subsets of peripheral blood mononuclear cells (PBMCs) stimulated by S protein in vitro and discussed the potential of the mechanism transforming effector $CD8^+$ T cells into memory $CD8^+$ T cells as a treatment strategy in SARS-CoV-2 infection.

Results

Preparation and activity identification of S1 and S2 proteins. S protein is the most important SARS-CoV-2 surface protein, and is related to the infectious capacity of the virus. Studies of the structure and function of S protein advance understanding of the mechanisms of viral invasion and pathogenicity. S protein forms a corolla-like structure in the form of a trimer, which is cleaved into two subunits, S1 and S2, under the action of host cell proteases. S1 mainly contains the receptor-binding domain, which is responsible for identifying cellular receptors. S2 contains the basic components required for the membrane fusion process. The main functions of S protein and its research significance are as follows: S protein mediates binding between virus and host cell membrane receptors and membrane fusion, S protein determines the host range and specificity of the virus, and S protein is an important site for host immunity and vaccine design. As shown in Fig. 1, the purity of SARS-CoV-2 S protein (S1 and S2 subunits) cloned and expressed in *E. coli* was more than 95%. The effect of S protein on the proliferation of normal human PBMCs was observed by the MTT assay. The results showed that S protein stimulates proliferation and cytokine secretion of PBMCs, indicating that S protein has the characteristics of an antigen.

Effect of vMIP-Ⅱ on the total number and classification of lymphatic cells in patients with SARS-CoV-2. This study included patients at Wuhan Union Medical College Hospital (Fangzhou Hospital) and Nanyang First People's Hospital with clinical symptoms including fever, cough, and chest tightness (but without respiratory failure or intubation). Clinical symptoms improved significantly after one week of vMIP-II treatment. Temperatures were normal, coughs reduced, and chest tightness became mild. Routine blood, biochemical blood, and lung CT scans before and one week after vMIP-II treatment showed the ground glass lesions and white areas of the lungs were significantly alleviated, while peripheral blood

component examinations showed significant increases in the total numbers and proportions of lymphocytes (Table. 1 and Fig. 2a). Compared with those of patients receiving symptomatic treatment (non-vMIP-II), clinical symptoms were significantly reduced. The median time for the virus to turn negative was 16 days, which was significantly shorter than that in the symptomatic treatment group (22 days)[3].

Responsiveness of blood PBMCs to S protein in recovering patients. The classification of $CD8^+$ T cell subgroups based on the PBMCs of convalescent patients showed that the ratios of T_{CM} cells in the vMIP-II treatment and asymptomatic infection groups were significantly higher than that in the symptomatic infection group, although there was no significant difference in the total number of lymphocytes (Table. 2, Fig. 2b).

The effects of S protein on the cytokine production levels in different groups of PBMCs were examined in convalescent patients after one week of testing negative for viral infection. The different groups of separated PBMCs were treated with S protein (100 ng/mL S1+ S2 protein at a ratio of 2:1) and detected by using a cytokine kit, *p-value 0.05. There were also differences in the cytokine secretion of PBMCs co-incubated with S protein and vMIP-II among the three groups of patients. After 6 h of S protein (100 ng/mL) stimulation, cytokine secretion in the vMIP-II treatment group and the asymptomatic infection group was stronger than that in the control group (p-value < 0.05) (Fig. 2c). When S protein and vMIP-II (50 ng/mL) were administered together, the cell proliferation curve tended to be more durable. Similarly, the recovery period in the vMIP-II group showed more persistent cell proliferation (Fig. 2d).

The results showed significantly more memory subset PBMCs in the vMIP-II treatment group and asymptomatic infection group than in the control group. Correspondingly, the cell proliferation rate of PBMCs cultured in vitro and stimulated by S protein was consistent with the level of memory $CD8^+$ T cells. This suggests that the memory $CD8^+$ T level is related to antiviral ability.

Both the use of vMIP-II in our clinical patients and the studies of convalescent blood samples showed that the numbers of $CD4^+$ T cells in the vMIP-II treatment group and the asymptomatic infection group were higher than that in the control diseased group (p-value < 0.05). There were more $CD45RA^+CD4^+$ T cells in the vMIP-II treatment group than in the other two groups, but there was no significant difference between the sizes of $CD45RA^+$ subgroups in the asymptomatic infection group and control group. In contrast, the proportion of $CD45RO^+$ subgroups of $CD8^+$ T cells in the vMIP-II treatment group and asymptomatic group was higher than that in the control group, and the proportion of T_{CM} subgroups in $CD45RO^+$ T cell increased significantly. These results show that the level of T_{CM} subgroups of $CD8^+$ T cells may play a major role in defending against infection by SARS-CoV-2, and it is enhanced in the presence of vMIP-II. vMIP-II may reconstruct specific cellular immunity after infection by regulating the level of T_{CM} subgroups of $CD8^+$ T cells.

Surface molecule analysis of the $CD8^+$ T cell subgroup. $CD8^+$ T lymphocyte subgroup analysis on PBMCs treated with S protein and vMIP- was performed. As Table. 3 and Fig. 3a–b, the number of $CD8^+$ T_{CM}

cells remained low in the S protein control group, accounting for only approximately 8.19%. In the three vMIP-II treatment groups, there was no significant change in the total number of memory $CD8^+$ T cells, but it is interesting that the changes in the numbers of $CD8^+$ T_{CM} cells and effector $CD8^+$ T cells were significantly different. The proportion of T_{CM} cells increased significantly, and the proportion of T_{EM} cells decreased significantly, both in a dose-dependent manner. In addition, T_{EX} cells in the vMIP-II treatment group were significantly reduced compared to levels in the S protein group. This suggests that under vMIP-II treatment, effector $CD8^+$ T cells may change into memory $CD8^+$ T cells during the contraction phase of effector $CD8^+$ T cells, which may be related to the increase in the numbers of T_{CM} cells. The decrease in $CD8^+$ T_{EX} cells indicates either that the number of apoptotic cells decreased or that proliferation ability was enhanced. The above results suggest that vMIP-II has an impact on the differentiation of $CD8^+$ T cells, but the specific mechanism needs further research.

Cytokine detection of $CD8^+$ T cells. Through flow cytometry, we found that the secretion of cytokines from $CD8^+$ T cells was changed (Fig. 3c). The cytokines INF-γ, TNF-α, IL-2, IL-4, and granulysin, produced by different groups of $CD8^+$ T cells, were detected. In the S protein and S protein + vMIP-II groups, Th1 cytokines (INF-γ, IL-2) were significantly increased. TNF-α and IL-4 levels were also significantly increased in the S protein group, and significantly decreased in the S protein/vMIP-II co-incubation groups compared with levels in the control group. There were no significant differences in granulysin levels among the groups. These results show that $CD8^+$ T cells maintained their corresponding levels of effector activation in the presence of vMIP-II. The detection of these cytokines also confirmed that vMIP-II regulates the function of $CD8^+$ T cell subsets.

Differential $CD8^+$ T cell gene expression in the S protein and S + vMIP-II group. We applied RNA-seq to detect differential $CD8^+$ T cell gene expression in the 100 ng/mL vMIP-II treatment group (S protein + vMIP-II group) and the S protein group (which received no vMIP-II treatment). A total of 97 significantly differentially expressed genes were screened by the standard (fold difference ≥ 2, *p*-value < 0.01), including 48 that were significantly up-regulated and 31 significantly down-regulated (Fig. 4a).

Gene ontology analysis. The differentially expressed genes were subjected to GO ontology analysis. The results show (Table. 4, 5, S1) that the main biological processes the genes were involved in were cell differentiation, apoptosis, cell localization and metabolism, and phosphorylation. The main cellular components were the mitochondrion, and membrane component, among others. The main molecular functions were signaling pathway molecule, transmembrane receptor regulatory protein, and transcription factor activity, among others. Thus, vMIP-□ is mainly involved in regulation of the phosphorylation signaling pathway, cell movement, anti-apoptosis, and chemokine receptors in effector $CD8^+$ T cells in PBMCs stimulated by S protein, especially in regulation of the phosphorylation signaling pathway of chemokine receptors, which affects $CD8^+$ T_{CM} cell differentiation. The large-scale enrichment of differentially expressed genes involved in in signaling pathway molecules, transcription factor activity, and cell energy metabolism after vMIP-II treatment supports this idea.

KEGG pathway analysis of differentially expressed genes. We have annotated the KEGG biological pathways online for the differential genes and found that they are mainly enriched in the apoptotic pathway, the capacity metabolism (TCA cycle) pathway, the phosphorylation pathway, and some cell signaling pathways (Fig. 4b). After comprehensively analyzing the composition and proportions of the differentially expressed genes, we conclude that the most enriched pathway associated with effector $CD8^+$ T cells is the phosphorylation signaling pathway.

Identifying candidate differentially expressed genes. According to the results of gene ontology analysis, the phosphorylation pathway, TCA cycle, and regulation of apoptosis are the three GO-terms with the most significant enrichment of differentially expressed genes. We sorted the differential expression folds of genes involved in these 3 groups of biological processes in descending order from largest to smallest, and then selected the differentially expressed genes with fold differences > 3 (p-value < 0.001; $\log_2$ ratio > 1.5). Ultimately, *GNAT1*, *PI3K*, *ERK*, *AKT*, *NF-κB*, *BCL-2*, *FAS*, *CXCR4*, *CX3CR1*, *CCR5*, *CCR7*, *PK*, and *PFK-1* were identified as key target genes for our subsequent research.

RT-PCR detection. We reverse-checked these 13 genes with qRT-PCR, and the results are shown in Fig. 4c. Compared to that in the effector $CD8^+$ T cells of the S protein and S + vMIP-II (100 ng/ml) groups, the expression of *CXCR4*, *CCR5*, *CX3CR1*, *PFK-1*, *GNAT1*, *PI3K*, *ERK*, *BCL-2*, and *AKT* in the vMIP-II-treated group were all significantly reduced, while the expression of *CCR7*, *PK*, *FAS*, and *NF-κB* increased significantly, which is consistent with the up-regulation and down-regulation results of RNA-seq.

Effect of vMIP-Ⅱ on Giα of effector $CD8^+$ T cells. Our gene sequencing and qRT-PCR results show that Gi protein α in CD8+ T cells is affected by vMIP-Ⅱ. Therefore, we performed western blotting to determine whether vMIP-II affects Gi protein receptor α in $CD8^+$ T cells. The results showed that compared with that in the S protein group, the expression of Gi protein receptor α in $CD8^+$ T cells treated with vMIP-Ⅱ was significantly inhibited (Fig. 5a), indicating that vMIP-Ⅱ affects differentiation of effector $CD8^+$ T_{CM} subgroups through the G protein signaling pathway and chemokine receptors.

To further understand the importance of G protein to the effects of vMIP-Ⅱ, Gi α antisense oligodeoxynucleotides were used. Fig. 5a shows that Giα antisense oligodeoxynucleotides significantly reduced the expression of G protein, indicating the effective activity of antisense RNA on Giα. When the S protein group was treated with Giα antisense oligodeoxynucleotides, and then treated with vMIP-Ⅱ (100 ng/mL), there was no obvious change in T_{CM} subgroup differentiation as detected by flow cytometry.

vMIP-II decreases rapid calcium influx. The effect of vMIP-II on intracellular rapid calcium ion concentration was detected continuously and dynamically in a time-resolved assay. hMIP-1Ⅱ (50 ng/mL) was administered to positive stimulated cells to cause a sharp increase in intracellular calcium ion concentrations. vMIP-II stimulation (100 ng/mL) did not increase the amplitude of intracellular calcium ion concentration (Fig. 5b), and the speed of calcium ion inflow stabilized at a lower level.

vMIP-II-induced calcium release from intracellular calcium ion pools

As shown in Fig. 5c, when vMIP-II was co-cultured with EDTA, EDTA chelated out extracellular calcium ions, but weak calcium ions could still be detected in the cell, indicating that vMIP-II induces calcium release from intracellular calcium ion pools.

Effect of vMIP-Ⅱ on mitochondrial membrane potential in effector $CD8^+$ T cells

The most intuitive manifestation of mitochondrial dysfunction in cells is the decrease of mitochondrial membrane potential. To detect the effect of vMIP-II on mitochondrial function in $CD8^+$ T cells, we detected changes in mitochondrial membrane potential in S protein-treated $CD8^+$ T cells (Fig. 5d). The JC-1 fluorescent probe is widely used in the determination of mitochondrial membrane potential. When potential is high, the probe gathers in the mitochondrial matrix and forms a polymer to produce red fluorescence. Conversely, JC-1 exists as a monomer and generates green fluorescence when membrane potential is low. The experimental results are shown in the figure below. The greater degree of red fluorescence after vMIP-II treatment shows that mitochondrial membrane potential was higher in the vMIP-II group than in the S protein control group (p-value < 0.01) (Fig. 5e).

Phosphorylation pathway analysis

$CD8^+$ T cells from the 100 ng/mL vMIP-II treatment group were cultured in 0.1% bovine serum culture medium for 1 h, and the S protein group not treated with vMIP-Ⅱ was used as a control. The expression levels of phosphorylated ERK1/2 and Akt proteins were detected 6 h after stimulation. The results in Fig. 5f show that high levels of phosphorylated ERK1/2 and Akt were detected in $CD8^+$ T cells only in the presence of S protein. In the presence of vMIP-II, the expression levels of phosphorylated ERK1/2 and Akt were significantly reduced. This indicates that vMIP-II inhibits expression of phosphorylated ERK1/2 and Akt proteins in the chemokine-receptor signaling pathway.

Discussion

Although the pathological mechanisms of COVID-19 are unclear, it is clear that the virus causes the body to produce a specific cellular immune response characterized by effector T cell-based immune exhaustion, causing inflammatory factor storms and inflammatory injury due to "suicide" of T cells. Severe and fatal cases are marked by lymphocyte overactivation and enhanced cytotoxicity without exception [3,4].

Our research shows that vMIP-II increases the body's specific $CD8^+$ T cell immune response, significantly improves the degree of lymphocyte reduction in patients, reduces the clinical symptoms of COVID-19, and significant shortens the amount of time before the virus turns negative. Due to restrictions aimed to control SARS-CoV-2 spread, there has been no analysis of lymphocyte subgroups in patients treated with vMIP-II. Thus, we isolated and cultured PBMCs and classified their subgroups in patients with a recovery period of one week when the virus became negative. The total numbers of $CD3^+$ T cells and $CD4^+$ T cells among the PBMCs of the vMIP-II and asymptomatic infection groups were significantly different from

those in the symptomatic control group (p-value < 0.05). The CD45RA$^+$ subgroup of CD4$^+$ T cells increased only in the vMIP-II group. Among the CD8$^+$ T cell subgroups, the percentage of CD8$^+$ T_{CM} cells increased significantly (p-value < 0.01) in the vMIP-II and asymptomatic groups. Correspondingly, the experiments using SARS-CoV-2 S protein to stimulate the PBMCs of patients in the recovery period also showed that Th1 cytokine levels in the vMIP-II group increased, while granulysin levels remained unchanged, leading to lasting cell proliferation ability in the vMIP-II treatment group. Interestingly, the PBMCs in the asymptomatic group showed cytokine types, changes in cell subgroup ratios, and sustained cell proliferation capacity similar to those in the vMIP-II treatment group. This strongly suggests that the persistent cellular immunity induced by vMIP-II may be similar to the natural antiviral mechanism in asymptomatic individuals, with both related to the formation of long-term memory CD8$^+$ T cells. These results also indicate that S protein contains specific antigenic peptides that evoke persistent T cell responses. The location of these peptides deserves further study. The increase in the naive subtype (CD45RA$^+$) of CD4$^+$ T cells may be related to stem cell mobilization caused by inhibition of the CXCR4 receptor by vMIP-II[29,30].

Our previous studies found that vMIP-II enhances Th1 cell function in the human lymphatic system and induces specific CD8$^+$ T cell proliferation, but long-term injection in vivo does not induce the human body to produce antibodies [13-15,31,32]. The route of administration (intravenous and nasal) of vMIP-II and its safety in the human body have also been studied, and it has been fully proven a safe, lowly immunogenic, small-molecule protein[33-35]. This preliminary study of vMIP-II as a treatment for COVID-19 showed its protective effect on COVID-19-induced lymphocyte reduction. This result is consistent with our previous report that vMIP-II has a significant protective effect on the reduction of lymphocytes caused by SIV and HIV infection[15,36]. Therefore, vMIP-II is a good immune reconstructing factor for acute viral infection.

We further explored the immune reconstructing mechanism of vMIP-II. T cells express different chemokine receptors at various stages of development, maturation, and activation, thus exerting different biological effects[37]. The expression of T cell-associated chemokines and their receptors has different phases and distributions in different T cell subgroups, and through the mode of specific binding of chemokines to their receptors, chemokines participate in the development of T cells and regulate directed migration of the cells, which affects the immune status of local tissue and even the entire body[38]. The interaction network between chemokines and their receptors is deeply interconnected. One chemokine can bind to multiple chemokine receptors, and one chemokine receptor can also have several high-affinity ligands. This fully reflects the complexity of interaction between chemokine receptors and their ligands[39]. A large number of early studies have confirmed that vMIP-II, encoded by the human herpesvirus 8 genome, is the only chemokine that can bind to three major classes of chemokine receptors (CCR, CXCR, and CX3CR)[40]. It is an antagonist of many chemokine receptors, competing with endogenous chemokines to reduce signal transduction of those receptors[41,42]. Although vMIP-II is widely recognized as a broad-spectrum chemokine receptor antagonist, when there are multiple chemokine receptors for

human T cells and multiple ligands for each receptor, there is complex diversity in their interactions[43]. Moreover, chemokine receptors are widely distributed in various subsets of T cells, and the downstream signaling pathways of each chemokine receptor may be different. As a result, the effect of vMIP-II on T lymphocytes cannot be easily judged by the binding characteristics of a single receptor.

In the present study, to further verify the reason for the increase in $CD8^+$ T_{CM} cells caused by vMIP-Ⅱ, we used Gene Ontology functional enrichment analysis to determine the overall effect of vMIP-II on $CD8^+$ T cells. The expression of chemokine receptors, such as CCR1, CCR5, CXCR4, and CX3CR1, decreased, while the expression of CCR7 increased and that of G protein decreased, indicating that vMIP-II has an effect on chemokine receptor expression. Notably, when the anti-sense oligonucleotide of G_i Ⅱ was used to knock down the function of G protein, the T_{CM} subgroup was reduced compared to the presence of vMIP-II, which fully demonstrates that vMIP-II works through the chemokine receptor pathway. Of course, it is currently difficult to determine whether the increased expression of CCR7 is directly caused by vMIP-II, induced by a decrease in the density of other receptors on the cell membrane, or caused only by natural ligand regulation of CCR7. In addition to chemokine receptors, significant differences were shown among transcription factors, oxidative phosphorylation function, and intracellular survival and proliferation-related kinases. Among them, the enhanced oxidative phosphorylation function indicates a certain change in the manner of cell energy metabolism, which is related effector $CD8^+$ T cells being mainly powered by glycolysis and memory T cells by mitochondria. It is worth noting that many apoptosis-related genes, such as *BLC-2* and *FAS,* were changed, indicating that the survival and proliferative capacity of effector $CD8^+$ T was enhanced, which is also one of the reasons for the changes in the numbers of $CD8^+$ subgroups. In general, the mechanism by which vMIP-II enhances the T_{CM} subgroup of $CD8^+$ T cells shows that metabolic reprogramming events, including inhibition of chemokine receptors and related signaling pathways of effector $CD8^+$ T cells and activation of their anti-apoptotic capacity and mitochondrial supply mode, change effector $CD8^+$ T cells into central memory $CD8^+$ T cells.

It has been reported that the T_{CM} cells of central long-term memory $CD8^+$ T cells are derived from a subset of T_{EM} cells, but the mechanism of this transformation is unclear[44,45]. Herein, we used vMIP-II studies to clearly demonstrate that the chemokine receptor-related phosphorylation pathway of effector $CD8^+$ T cells is significantly down-regulated (but CCR7 pathway activation is still retained), and while inhibiting the apoptotic pathway, these molecular mechanisms affect the fate of effector $CD8^+$ T cells, thereby increasing levels of central memory $CD8^+$ T cells.

Chiefly, after vMIP-II treatment, the functions and proportions of $CD8^+$ T cell subgroups in patients changed, and the proportions of central memory cells increased most obviously. The cause of this phenomenon may be the result of vMIP-II acting on multiple chemokine receptors. This led to a decrease in apoptotic gene expression and an up-regulation of survival proliferative genes associated with intracellular phosphorylation pathways, namely enhancing the proliferation capacity of effector $CD8^+$ T cells to dedifferentiated stem cells and promoting differentiation of $CD8^+$ T cells into memory subgroups.

It is well understood that COVID-19 greatly reduces the number of T lymphocytes and increases the number of exhausted $CD8^+$ T cells in patients. These findings not only provide effective therapeutic factors that might be exploited against SARS-CoV-2 infection but also a new strategy for cellular immune reconstitution following acute virus infection. However, as the interactions between chemokines and their receptor system is complicated, one or several chemokine receptors should be blocked in the future by gene-editing technology, and different knock-down combinations of chemokine receptors artificially made to further enrich the theory of reconstituting immune response after viral infection by modulating the stem capacity of effector $CD8^+$ T cells.

Methods

Cloning, Expression, and Purification of S1 and S2 Proteins. The S-protein of SARS-CoV-2 Guangzhou strain (GISAID: EPI-ISL-406533) occupies bases 21563–25384 of its genome, corresponding to 1273 amino acids, and encodes a protein of 141.2 kDa. Its cleavage activation site is YKTPPI, and it is cleaved into the S1 (25kDa) and S2 (58 kDa) subunits.

Using His-tagged pQE-TriSystem (Invitrogen) as a plasmid, the SARS-CoV-2 S1 and S2 subunit genes were amplified and recombined to obtain pQE-His SARS-CoV-2-S1 and pQE-His SARS-CoV-2-S2. The construction scheme is shown in Fig. S1. The plasmids were digested and sequenced for confirmation and transfected into *Escherichia coli M15* for culture. The speed and ventilation was controlled during bacterial fermentation culture, and dissolved oxygen was set ≥40%. When bacterial optical density (OD) as measured at OD_{600} = 0.8, the inducer IPTG (1 mM) was added. After fermentation, we collected bacteria, then added inclusion body lysis buffer and centrifuged for 10 min. The collected inclusion body supernatant was passed through an affinity Ni column to obtain crudely purified S1 and S2 proteins. The processed protein was loaded onto a Superdex-75 molecular sieve and a DEAE column in sequence and eluted with an elution buffer. The eluted peaks were collected to obtain purified S1 and S2 proteins. Purity was determined by HPLC.

Identification of S1 and S2 Protein Activity. For the isolation of PBMCs, lymphocytes were isolated according to the conventional method of peripheral blood lymphocyte separation. The cell concentration in RPMI1640 medium was adjusted to 2.5×10^6/mL, and 20 μL of 5 mg/mL MTT solution was added and incubated for 4 h. The supernatant was discarded, and 150 μL of DMSO was added to dissolve the precipitate. OD values were measured at 490 nm, and cell viability was calculated by the following formula: (%) = (OD treatment group/OD blank) × 100%. The experiment was performed in triplicate. Cells with viability > 90% were used in the following experiments.

After mixing the S1 and S2 proteins at a ratio of 2:1, the PBMCs were stimulated. Cells were seeded at 5×10^4/well in 96-well plates and incubated with S protein for 12 h to examine changes in morphology. Samples were divided into the blank control group, S protein stimulation group (10, 50, and 250 ng/mL), and PHA (2 μg/mL) group. There were three replicates within each group.

vMIP-II for the Treatment of SARS-CoV-2 Infection. This research was approved by the Ethics Committee of Union Hospital, Tongji Hospital of Huazhong University of Science and Technology (No. 2020-0006). Human peripheral blood samples were collected after obtaining informed consent and appropriate Institutional Review Board approval.

This study obtained blood samples from 15 patients, 10 of whom in Union Hospital (Wuhan, Hubei Province, China), had been clinically diagnosed with COVID-19, shown symptoms included fever, cough, and obvious changes in the lungs as visualized by CT, but no obvious respiratory failure. And 5 of whom in Nanyang People's Hospital (Nanyang, Henan Province, China), were positive for viral infection but had no fever, cough, or significant changes in lung X-rays. All patients with COVID-19 were given symptomatic treatment, such as rest, antibacterial and oxygen inhalation, according to the “Guidelines for the Diagnosis and Treatment of Novel Coronavirus (2019-nCoV) Infection by the National Health Commission (Trial Version 5)”. 5 patients in Union Hospital were randomly selected and given intravenous drip of vMIP-II in a single blind trial, as the vMIP-treatment group: lyophilized, each of powered vMIP-II at 250,000 active units/penicillin bottle(approximately 250 μg), dissolved in normal saline injected twice a day for 7 days was used as a course of treatment. Other 5 patients in Union Hospital with symptomatic treatment were divided into symptomatic group. The last 5patients in Nanyang People's Hospital were divided into asymptomatic group.

Blood samples were obtained at 7 days after patient’s blood tested negative for SARS-CoV-2. The blood samples were subjected to PBMC isolation, $CD8^+$ T cell subgroup sorting, and co-incubation experiments involving SARS-CoV-2 S protein and vMIP-II as described below.

Isolation of PBMCs. blood samples were mixed with 4 mL EDTA to prevent coagulation and centrifuged at 1500 rpm (centrifugation radius 10 cm) for 10 min. The upper plasma was extracted, and 3 mL of lymphocyte separation solution was added. The resulting mixture was centrifuged at 2500 rpm (centrifugation radius: 10 cm) for 20 min, and the supernatant was discarded. One milliliter of 1640 medium was added to resuspend 1×10^7 cells/mL. Isolated normal human PBMCs were divided into five groups: a blank control group, S protein group (100 μg of S1 + S2 protein at a the ratio of 2:1), and three vMIP-II treatment groups. The vMIP-II treatment group included group I (25 ng vMIP-II + S protein), group II (50 ng vMIP-II + S protein), and group III (100 μg vMIP-II + S protein). PBMCs cells were co-incubated with S protein and vMIP-II according to the above group doses. Each group was cultured in vitro for 6 h before use.

Subset Analysis of $CD3^+$, $CD4^+$, and $CD8^+$ T Cells Among PBMCs. Cultured cells (1.5 mL) were placed into test tubes, and 10 μL of each of four monoclonal fluorescent antibodies, including anti-human CD3-PE, CD4-FITC, CD8-APC, CD45RO-PE-Cy5, and CD62L- APC-H7 in T cells after sorting of anti-human CD3-PE (BD Biosciences, Franklin Lakes, NJ, USA) were added, and then mixed with an oscillator and stored in darkness for 15–30 min at room temperature (20–25 °C). Afterwards, 2 mL of hemolysin was added to dissolve red blood cells, and the cultures were mixed on an oscillator, stored at room temperature for 10 min in the dark, and then centrifuged at 1000 rpm for 10 min. The supernatant was discarded. Cells were

washed with 1 mL of PBS buffer containing 0.1% NaN_3 and centrifuged at 1000 rpm for 10 min. The supernatant was decanted. Fixative (300 μL) was added to resuspend the cells, which were then detected using a BD-FACsCalibur flow cytometer (BD Biosciences).

Flow Cytometric Sorting of $CD8^+$ T Cell Subtypes. Cultured cells (1.5 mL) were placed into two test tubes, and 10 μL of each of four monoclonal fluorescent antibodies, including anti-human CD3-PE, CD4-FITC, CD8-APC, CD45RO-PE-Cy5, and CD62L-APC-H7 in T cells after sorting of anti-human CD3-PE (BD Biosciences), was added into the first test tube, which was treated according to the method in 1.3.2 and sorted on the flow cytometer. CD45RA and CD62L were used to distinguish different subgroups of $CD8^+$ T cells: $CD45RA^+CD62L^+$ is the phenotype of naïve $CD8^+$ T cells (T_n cells), $CD45RA^+CD62L^-$ is the phenotype of effector $CD8^+$ T cells (T_E cells), $CD45RA^-CD62L^+$ is the phenotype of central memory $CD8^+$ T cells (T_{CM} cells); and $CD45RA^-CD62L^-$ is the phenotype of effector memory $CD8^+$ T cells (T_{EM} cells). In the second test tube, 10 μL of each of three kinds of monoclonal fluorescent antibodies, including CD8-APC, PD-1-PE, and Tim-3-APC-H7 (BD Biosciences), were applied in the same manner as above and sorted on the flow cytometer. The highly expressed inhibitory molecules PD-1 and Tim-3 were used to distinguish exhausted $CD8^+$ T cells (T_{EX} cells).

Cytokine Detection of Specific $CD8^+$ T Cells Induced by S Protein. Cultured cells (1.5 mL) were placed into a test tube, and PMA (50 mg/L), ionomycin (750 mg/L), and blocker BFA (1×) were added. Then the cells were incubated at 37 °C under 5% CO_2 for 6 h. Each group of cells was equally divided into five 1.5 mL centrifuge tubes and centrifuged at 1500 rpm for 5 min. The supernatant was discarded and the cells were washed with PBS. The flow cytometry surface antibody CD8-APC-Cy7 was added to the cells in the dark after the supernatant was discarded. The cells were incubated at 4 °C for 20 min in the dark. The cells were then fixed with 200 μL of 4% paraformaldehyde. After fixing at 4 °C in the dark for 30 min, each tube was centrifuged at 500 rpm for 5 min, and the supernatant was discarded. After 200 μL film-breaking agent was added, the cells were incubated at 4 ℃ in the dark for 1 h, and then centrifuged at 1500 rpm for 5 min. The supernatant was discarded. Five tubes from each group were protected from light, and intracellular antibodies, including IFN-γ-APC, TNF-α-APC, IL2-APC, IL4-APC, and granzyme-APC (BD Biosciences) were added to the tubes and incubated at 4 ℃ for 20 min . Flow cytometry was used to detect cytokine secretion.

RNA Sequencing. Transcriptome sequencing was performed by Shanghai Kangcheng Biotechnology Co., Ltd. (Shanghai, China) The sequencing platform used was Illumina Hiseq 2500 V4, the sequencing mode was 125PE, and the samples were RNA-seq libraries of $CD8^+$ T cell populations from the S protein group and 100 ng/mL vMIP-II/S protein group. Construction of RNA-seq library: total RNA was enriched with Oligo (dT). The RNA was randomly cut into 200 nt fragments, random primer hexamers were reverse transcribed into cDNA, end repair was performed, and adenine was added. After the adapter was added, PCR amplification enabled library construction.

Sample libraries were mixed according to Illumina standards to prepare clusters. One end of the replication chain was fixed on the chip, and the other end was randomly fixed to complement another nearby primer and form a "bridge." The single strand of the formed bridge used the surrounding primers as amplification primers, which were amplified on the surface of the chip to become double strands, and then denatured to single strands. The next round of the amplification reaction was then performed. After several rounds, each single molecule was amplified in large quantities to a cluster.

According to the quality control standard, short sequences containing linkers, short sequences with a proportion of N > 10%, and short sequences of low quality were removed. The remaining sequences (Q30 > 85%) were used for subsequent analysis.

Differential Gene Expression Analysis. Differential gene expression analysis of effector $CD8^+$ T cell samples in the 100 ng/mL vMIP-□ treatment group and S protein group was performed using the DESeq software. The P values of the results were controlled and adjusted using the methods of Benjamini and Hochberg. The adjusted *p*-value < 0.01 and the differential expression multiple > 2 ($|\log_2| > 1$) were selected by DESeq and labeled as differentially expressed genes.

Functional enrichment analysis of differentially expressed genes was performed using GOseq R software package and the Gene Ontology resource (http://www.geneontology.org/). KEGG is a database that contain mined molecular-level information, especially large-scale molecular datasets generated by genome sequencing and other high-throughput experimental techniques, on the advanced functions of biological systems, such as cells, organisms, and ecosystems (http://www.genome.jp/kegg/). Statistical enrichment analysis of differentially expressed genes in the KEGG pathway was performed using KOBAS software. Pathway enrichment analysis of differentially expressed genes was used to analyze whether genes were over-represented in certain pathways, and gene enrichment factors were used to analyze the degree of pathway enrichment.

RT-PCR. To verify the accuracy of the RNA-seq data, we selected some differentially expressed genes and performed relative fluorescence quantitative PCR analysis on their expression levels. Sorted $CD8^+$ T cells were placed in a 5% CO_2 cell incubator and cultured at 37 °C for 24 h. $CD8^+$ T cell total RNA extraction was performed according to the cell total RNA extraction kit instructions, and a SuperScript™ Preamplification System for First Strand cDNA Synthesis kit was used for cDNA synthesis. All primer sequences used in the real-time PCR reaction are listed in Table. S4. The reaction was performed in a real-time PCR machine (MiniOpticon; Bio-Rad, Hercules, CA, USA) according to the manufacturer's instructions. The total reaction volume was 25.0 μL, including 2.0 μL of total RNA, 8.5 μL of RNase-free H_2O, 0.5 μL each of the forward and reverse primers (10 mM/L), 12.5 μL 2× One-step SYBR RT-PCR Buffer □, 0.5 μL TaKaRa Ex Taq HS (5 U/μL), and 0.5 μL PrimeScript RT Enzyme Mix II. The PCR reaction was performed at 95 °C for 5 min, 95 °C for 30 s, 60 °C for 45 s, and 72 °C for 45 s, for a total of 33 cycles. All experiments were performed in 3 independent biological replicates. Standard relative transcription levels were estimated using the $2^{-\Delta\Delta Ct}$ method.

Western Blot. $CD8^+$ T cells selected from the 100 ng/mL vMIP-II treatment group and S protein group were sonicated and centrifuged for 10 min, and the supernatant was collected and the pellet discarded. The supernatant was subjected to SDS-PAGE electrophoresis. After the electrophoretic band was obtained, a strip with a molecular weight of 45 kd was cut and transferred to the membrane. The membrane was stained with 1 × Polysine red staining solution for 5 min. After being washed with water, the membrane was dried for use. After the membrane was wetted with TBS from the bottom to the top, it was transferred to a plate containing a blocking solution and shaken for 1 h at room temperature on a decolorization shaker. The primary antibody Anti-GNAO1 (Abcam, Cambridge, UK) was diluted to the appropriate concentration with TBST and added to the membrane. After incubation at room temperature for 1–2 hours, the membrane was washed with TBST twice at room temperature on a shaker for 10 min and then washed again with TBS for 10 min. A goat anti-rabbit Ig G-HRP dilution was then prepared and applied to the membrane. After being incubated at room temperature for 1–2 hours, the membrane was washed with TBST at room temperature twice on a shaker for 10 min each time and blotted dry. The membrane was then combined with the film. The tablet was pressed for 1 min and developed for 30 s. The membrane was then washed with water, allowed to dry, and then scanned further. ImageJ2x was used to determine the gray value of the internal reference gene and the target gene.

Treatment with Antisense RNA for G Protein α Subunit. The S protein group was treated with antisense RNA for G protein α subunit, and then with vMIP-Ⅱ (100 ng/mL). $CD8^+$ T cell subsets were detected by flow cytometry. The antisense oligonucleotide sequence of G_i α mRNA (ODN) is 5'-ATG GTC AGC CCA GAG CCT CCG GAT GAC GCC CGA-3', a phosphorothioate oligonucleotide synthesized by Takara Bio (Kusatsu, Japan). $CD8^+$ T cells were divided into four groups: the G_iα At-RNA group, S protein, S protein + G_iα At-RNA group, and S protein + G_iα At-RNA + vMIP-Ⅱ group. $CD8^+$ T cells were added to 96-well cell culture plates at 100 μL/well and cultured in an incubator at 37 °C under 5% CO_2. G_i α ODN was added according to grouping 1 h after adding S protein, and vMIP-II 1 h after adding G_i α ODN. Cells were collected after 8 h for flow cytometric sorting of $CD8^+$ T cell subtypes.

Intracellular Calcium Ion Concentration. Measurement of vMIP-II-induced rapid calcium influx and vMIP-II-induced calcium release from the intracellular calcium ion pool were performed separately. The former experiment was divided into 3 groups, with vMIP-II concentrations of 25 ng/mL, 50 ng/mL, and 100 ng/mL; the latter experiment was divided into 2 groups, with EDTA-containing and EDTA-free background solutions. All experiments were performed in triplicate holes. Cells were loaded with Fluo-3/AM, and 2 mL of cell suspension was added to each cuvette. Cuvettes were equilibrated at 37 °C for 5 min, and the excited with 488 nm UV light. The emitted light was detected at 525 nm. After reached baseline within 1–2 minutes, vMIP-II was added to the cells. The detection parameters of the fluorescence spectrophotometer were set, and the data interval was 0.1 min or 0.1 s. After 10 min of detection, data collection was stopped and a curve was drawn.

JC-1 Staining. The measurement of mitochondrial membrane potential was performed with a JC-1 kit (Shanghai Biyuntian Co., Shanghai, China) according to the manufacturer's instructions. After the culture

medium was removed from the cells, the cells were washed once with PBS. Afterwards, 1 mL of cell culture solution and 0.5 mL of JC-1 staining working solution were added to the cells. After being shaken well, the cells were incubated at 37 ° C for 20 min. Afterwards, the supernatant was removed, then the cells were washed twice with diluted JC-1 staining buffer (1×). Cell culture solution (2 mL) was added to the washed cells, and the cells were observed under a fluorescence microscope.

Cellular Phosphorylated Protein Levels. The effector $CD8^+$ T cells sorted from the PBMCs were starved in 0.1% bovine serum RPMI 1640 medium for 1 h and stimulated with or without CCL21 (200 ng/mL). The cells were then collected and washed 3 times with cold PBS. Total protein was extracted after the cells were lysed, quantified by the Bradford method, and denatured by heating. SDS-PAGE was performed on the equal amounts of protein. The proteins were transferred to a PVDF membrane and blocked overnight with 5% skim milk powder formulated with TBS overnight. Rabbit anti-phosphorylated Akt (1:1000), Akt (1:1000), and ERK1/2 (1:1000) primary antibodies were added to the membrane and incubated at room temperature for 2 h. The membrane was then washed with TTBS (TBS with 1 part per thousand Tween-20). The HRP-sheep anti-rabbit IgG secondary antibody (1:2000) was incubated for 1 h at room temperature. After being washing with TBST solution, the membrane was treated with luminescent solution for 3 min, blotted dry, and analyzed after developing. The gray value of the internal reference gene and the target genes were determined using ImageJ2x.

Statistics. All numerical data are presented as the mean ± SD (standard deviations). The statistical significance of all in vivo and in vitro studies was determined among three or more biological replicates using Prism software. A two-tailed t-test was used to determine the *p*-value.

Declarations

Data availability

All data are present in this study. Questions and requests for SARS-CoV-2 patients' lung CT scans can be made to H.S.

Acknowledgements

This work was funded by National Key R&D Program of China(2017YFC1103400), National Natural Science Foundation of China (NSFC, NO.3087221), National Natural Science Foundation of China (NSFC, NO.81473454), Natural Science Foundation of Guangdong Province, China (2015A030313331) and Guangzhou Soyoung Biotechnology Company.

Author contributions

H.S. and W.H. conceived the project. H.S., A.X., N.Z., Z.J. designed the experiments. Y.G., B.H., L.F., S.Z., N.Z. conducted clinical trials, All authors performed the experiments. S.L., Y.W., Z.J. performed data analysis, and wrote the manuscript with input from all coauthors.

Competing interests

The authors declare no competing interests.

Additional information

Supplementary information is available for this paper online

Correspondence and requests for materials should be addressed to H.S.

References

1. Chan, J. F. W. et al. A familial cluster of pneumoniaassociated with the 2019 novel coronavirus indicating person-to-persontransmission: a study of a family cluster. *Lancet* **395,** 514-523 (2020).
2. Wu, J. T., Leung, K. & Leung, G. M. Nowcasting and forecasting the potentialdomestic and international spread of the 2019-nCoV outbreak originatingin Wuhan, China: a modelling study. *Lancet* **395,** 689-697(2020).
3. Zhou, F. et al. Clinical course and risk factors for mortality of adult inpatients with COVID-19 in Wuhan, China: a retrospective cohort study. *Lancet* **395,** 1054-1062 (2020).
4. Xu, Z. et al. Pathological findings of COVID-19 associated with acute respiratory distress syndrome. *Lancet Respir Med*. **8,** 420-422 (2020).
5. Cao, X. COVID-19: immunopathology and its implications for therapy. *Nat. Rev. Immunol*. **20,** 269-270 (2020).
6. Liu, S. et al. Screening and mechanism of antagonist peptide for CC chemokine receptor 1 (CCR1) derived from viral macrophage inflammatory protein II. *Trop. J. Pharm. Res*. **13,** 697 (2014).
7. Kledal, T. N. et al. A broad-spectrum chemokine antagonist encoded by Kaposi's sarcoma-associated herpesvirus. *Science* **277,** 1656-1659 (1997).
8. Nakano, K. et al. Kaposi's sarcoma-associated herpesvirus (KSHV)-encoded vMIP-I and vMIP-II induce signal transduction and chemotaxis in monocytic cells. *Arch. Virol*. **148,** 871-890 (2003).
9. Dairaghi, D. J., Fan, R. A., McMaster, B. E., Hanley, M. R. & Schall, T. J. HHV8-encoded vMIP-I selectively engages chemokine receptor CCR8. Agonist and antagonist profiles of viral chemokines. *J. Biol. Chem*. **274,** 21569-21574 (1999).
10. Pawig, L., Klasen, C., Weber, C., Bernhagen, J. & Noels. H. Diversity and Inter-Connections in the CXCR4 Chemokine Receptor/Ligand Family: Molecular Perspectives. *Front. Immunol*. **6,** 429 (2015).
11. Chen, S. et al. In vivo inhibition of CC and CX3C chemokine-induced leukocyte infiltration and attenuation of glomerulonephritis in Wistar-Kyoto (WKY) rats by vMIP-II. *J. Exp. Med*. **188,** 193-198 (1998).
12. An, G. et al. Synthetic polypeptide derived from viral macrophage inflammatory protein II inhibit the uninfected CD4+ T cells apoptosis induced by HIV-1 extracellular nef. *Trop. J. Pharm. Res*. **13,** 683-

688 (2014).

13. Renne, R. et al. Experimental transmission of Kaposi's sarcoma-associated herpesvirus (KSHV/HHV-8) to SIV-positive and SIV-negative rhesus macaques. *J. Med. Primatol.* **33,** 1-9 (2004).
14. Sun, H. et al. Long-term intravenous administration of recombinant viral inflammatory protein-□ intensifies immune system of Cynomolgus macaque. *Chin. J. Immunol.* **23,** 11-15 (2007).
15. Guo, Q. et al. Effects of vMIP-□ on TCRVβ gene expression in SIV-infected MacacaFascicularis. *Chin. J. Immunol.* **22,** 604-607 (2006).
16. Ding, Q. et al. HIV-1 Coreceptor CXCR4 Antagonists Promote Clonal Expansion of Viral Epitope-Specific CD8+ T Cells During Acute SIV Infection in Rhesus Monkeys In Vivo. *J. Acquir. Immune. Defic. Syndr.* **69,** 145-53 (2015).
17. Fehr, A. R. & Perlman. S. Coronaviruses: an overview of their replication and pathogenesis. *MethodsMol. Biol.* **1282,** 1-23 (2015).
18. Gao, W. et al. Effects of a SARS-associated coronavirus vaccine in monkeys. *Lancet* **362,** 1895-1896 (2003).
19. Bukreyev, A. et al. Mucosal immunisation of African green monkeys (Cercopithecus aethiops) with an attenuated parainfluenza virus expressing the SARS coronavirus spike protein for the prevention of SARS. *Lancet* **363,** 2122-2127 (2004).
20. Du, L. et al. Identification of a receptor-binding domain in the S protein of the novel human coronavirus Middle East respiratory syndrome coronavirus as an essential target for vaccine development. *J. Virol.* **87,** 9939-9942 (2013).
21. The Coalition for Epidemic Preparedness Innovations. CEPI to fund three programmes to develop vaccines against the novel coronavirus, nCoV-2019. https://cepi. net/news_cepi/cepi-to-fund-three-programmes-to-developvaccines- against-the-novel-coronavirus-ncov-2019/ (2020).
22. Gerlach, C. et al. Heterogeneous differentiation patterns of individual CD8+T cells. *Science* **340,** 635-639 (2013).
23. Carbone, F. R, Mackay, L., Heath, W. R & Gebhardt, T. Distinct resident and recirculating memory T cell subsets in non-lymphoid tissues. *Curr. Opin. Immunol.* **25,** 329-333 (2013).
24. Mueller, S. N, Gebhardt, T., Carbone, F. R & Heath, W. R. Memory T cell subsets, migration patterns, and tissue residence. *Annu. Rev. Immunol.* **31,** 137-161 (2013).
25. Gebhardt, T., Mueller, S. N., Heath, W. R. & Carbone, F. R. Peripheral tissue surveillance and residency by memory T cells. *Trends Immunol.* **34,** 27-32 (2013).
26. Buchholz, V. R et al. Disparate individual fates compose robust CD8+ T cell immunity. *Science* **340,** 630-635 (2013).
27. Li, H. et al. Research progress on coronavirus and its therapeutic drugs. *Pharm. J. Chin.* 1-22 (2020).
28. Xie, X. et al.An infectious cDNA clone of SARS-CoV-2. *Cell Host Microbe.* **27,** 1-8 (2020).

29. Singh, P., Mohammad, K. S. & Pelus, L. M.. CXCR4 expression in the bone marrow microenvironment is required for hematopoietic stem and progenitor cell maintenance and early hematopoietic regeneration after myeloablation. *Stem Cells*. https://doi.org/10.1002/stem.3174 (2020).

30. Tang, Y., Wei, Y., Hu, S. & Zhang, H. SDF-1-CXCR4 Axis and Stem Cell Therapy of the Ischemic Heart Disease.*Basic Clin.Med*. **26,** 915-921 (2006).

31. Mo, X. & Sun, H. The anti-inflammatory effect of the CXCR4 antagonist-N15P peptide and its modulation on inflammation-associated mediators in LPS-induced PBMC.*Inflammation* **38,**1374-1383 (2015).

32. 32. Yang, Y. et al. Prediction of novel genes associated with negativeregulators of toll-like receptors-induced inflammation based on endotoxintolerance. *Inflammation* **35,**1889-1899 (2012).

33. Mo, X., Sun, H., Jia, Z., Li, X. & Zhang, G. Expression of Viral Macrophage Inflammatory Protein-inPichiapastoris and Its Anti-HIV-1 Activity. *Chin. J. Biol*. 24, 629-633 (2011).

34. Wang, F., Li, X., Mo, X., Zhang, G. & Sun, H. Abiologically active vMIP-II-IgG3-TfN fusion protein, secreted frommethylotrophic yeast Pichia pastoris. *Protein Expres. Purif*. 87,47–54 (2013).

35. Mo, X. et al. Pharmacokinetics and Tissue Distribution of Recombinant vMIP in Rats.*Chin. Pharm. J.* **11,** 852-854 (2008).

36. Mo, X., Ye, S., Zhang, G. & Sun, H. Anti-SIV Potency of a Broad Spectrum Chemokine Receptors Inhibitor,vMIP-II in vivo. *Virol. Sin*. 20, 459-463 (2005).

37. Strazza, M. & Mor, A. Consider the chemokines: a review of the interplay between chemokines and T cell subset function.Discov. *Med*. **24,** 31-39 (2017).

38. Miyabe, Y., Lian, J., Miyabe, C. & Luster, A. D. Chemokines in rheumatic diseases: pathogenic role and therapeutic implications. *Nat. Rev. Rheumatol*. **15,** 731-746 (2019).

39. Arimont, M. et al. Structural Analysis of Chemokine Receptor–Ligand Interactions.*Med. Chem*. **60,** 4735-4779 (2017).

40. Ye, S. et al. Analysis of receptor-binding properties of vMIP-. *Chin. J. Mod. Med*. **16,** 3546-3548 (2006).

41. Hua, X. et al. Internalization and modulation of the surface chemokine receptor CXCR4 induced by viral macrophage inflammatory protein-II. *Curr. Immunol*. **26,** 213-216 (2006).

42. Szpakowska, & Chevigné, A. vCCL2/vMIP-II, the viral master KEYmokine. *J. Leukoc. Biol*. **99,** 893-900 (2016).

43. Pawig, L., Klasen, C., Weber, C., Bernhagen, J. & Noels, H. Diversity and Inter-Connections in the CXCR4 Chemokine Receptor/Ligand Family: Molecular Perspectives. *Front.Immunol*. **6,** 429 (2015).

44. Gonzalez, S. M., Taborda , N. A. & Rugelesa, M. T. Role of Different Subpopulations of CD8+ T Cells during HIV Exposure and Infection. *Front. Immunol*. **8,** 936 (2017).

45. Akondy, R. S. et al. Origin and differentiation of human memory CD8 T cells after vaccination. *Nature* **552,** 362-367 (2017).

Tables

Table 1 Changes in peripheral blood lymphocytes of patients after continuous vMIP-Ⅱ treatment for 1 week (Mean ± SD, n = 5)

Groups	Enrollment			After treatment		
	Total Leucocyte Count (10^9/L)	Total Lymphocyte Count (10^9/L)	D dimer (mg/L)	Total Leucocyte Count (10^9/L)	Total Lymphocyte Count (10^9/L)	D dimer (mg/L)
vMIP-II treatment	6.74±1.93	0.90±1.21	1.94±0.17	7.09±2.08	1.51±1.17*	0.85±0.07*
Symptomatic treatment	7.27±1.68	0.83±1.15	2.08±0.21	7.68±1.72	1.28±2.23	0.99±0.09

Note: * p-value < 0.05 compared with the symptomatic treatment group; ** p-value < 0.01 compared with the symptomatic treatment group.

Table 2 Analysis of T subpopulations in PBMCs of recovery patients

Project	Diseased group (%)	Asymptomatic group (%)	vMIP-II treatment group (%)
Lymphocyte	30.9±3.86	34.2±4.59	35.8±5.14
$CD3^+$/Lymphocyte	60.1±6.22	70.2±7.28*	69.4±6.68*
$CD3^+CD4^+$	33.3±6.12	39.2±7.62*	38.5±6.27*
$CD3^+CD8^+$	25.4±7.55	27.4±8.41	26.5±7.83
$CD45RA^+$/CD4	47.3±10.2	55.9±9.62*	50.6±9.13
$CD45RO^+$/CD4	50.2±9.27	44.3±8.8	48.3±9.61
$CD4^+T_{CM}$	13.1±2.41	8.7±3.15	11.9±2.21
$CD4^+T_{EM}$	38.4±3.15	36.2±3.22	37.1±5.66
$CD45RA^+$/CD8	49.1±7.19	37.2±9.17*	35.2±7.66*
$CD45RO^+$/CD8	52.8±8.33	61.8±8.42*	63.8±9.34*
$CD8^+T_{CM}$	7.12±2.12	14.3±5.12**	17.1±4.12**
$CD8^+T_{EM}$	41.9±5.22	48.6±6.31*	47.6±7.22*

Note: Compared with the common symptomatic group, * *p*-value 0.05; ** *p*-value 0.01

Table 3 Changes in the subsets of memory $CD8^+$T cells (%. Mean ± SD. n=3)

Treatment	Memory$CD8^+$ T	Percentage of $CD8^+$Tcm	Percentage of $CD8^+$ Tem	Percentage of $CD8^+$ T_{EX}
Untreated control	73.99 ± 4.56	9.33 ± 4.54	86.20 ± 5.18	4.05 ± 1.17
25ng/ml	73.92 ±3.33	17.22 ± 2.75*	81.53 ± 6.17	6.83 ± 1.12*
50ng/ml	71.01 ± 4.63	23.85 ± 4.12**	75.17 ± 6.44	5.18 ± 1.18*
100 ng/ml	70.18 ± 3.45	29.39 ± 2.44**	71.19 ± 5.45	3.85 ± 1.69**
Sprotein(100ng/ml)	66.30 ± 2.56	8.19 ±1.48	89.33 ± 7.62	12.94 ± 1.88*

Note: Compared with the control group,* *p*-value0.05, ** *p*-value0.01

Table 4 Gene ontology analysis for significantly altered genes-biological process

Biological Progress	Count	*P*-value
Phosphorylation process	20	3.3E-06
Cell apoptosis	15	4.8E-04
Cell differentiation	11	6.1E-04
Glucose metabolic process	9	1.2E-03
Cell localization and metabolism	9	3.4E-03
Regulation of transcription, DNA-templated	9	5.3E-03
Regulation of mitophagy	7	4.1E-03
Cellular response to mechanical stimulus	6	2.8E-02
Systerm process	6	3.2E-02
Transcription from RNA polymerase II promoter	5	3.8E-02

Table 5 Gene ontology analysis for significantly altered genes-cellular component

Cellular Component	Count	*p*-value
Cytoplasm	26	5.3E-03
Intracellular membrane-bounded organelle	16	2.8E-04
Endoplasmic reticulum	12	4.5E-04
Mitochondrion	12	6.2E-04
Extracellular exosome	11	3.1E-03
Nucleoplasm	10	3.3E-03
ER to Golgi transport vesicle membrane	6	1.2E-02
RNA polymerase II transcription factor complex	6	3.1E-02
Receptor complex	5	2.8E-02
Peroxisome	4	6.1E-02

Figures

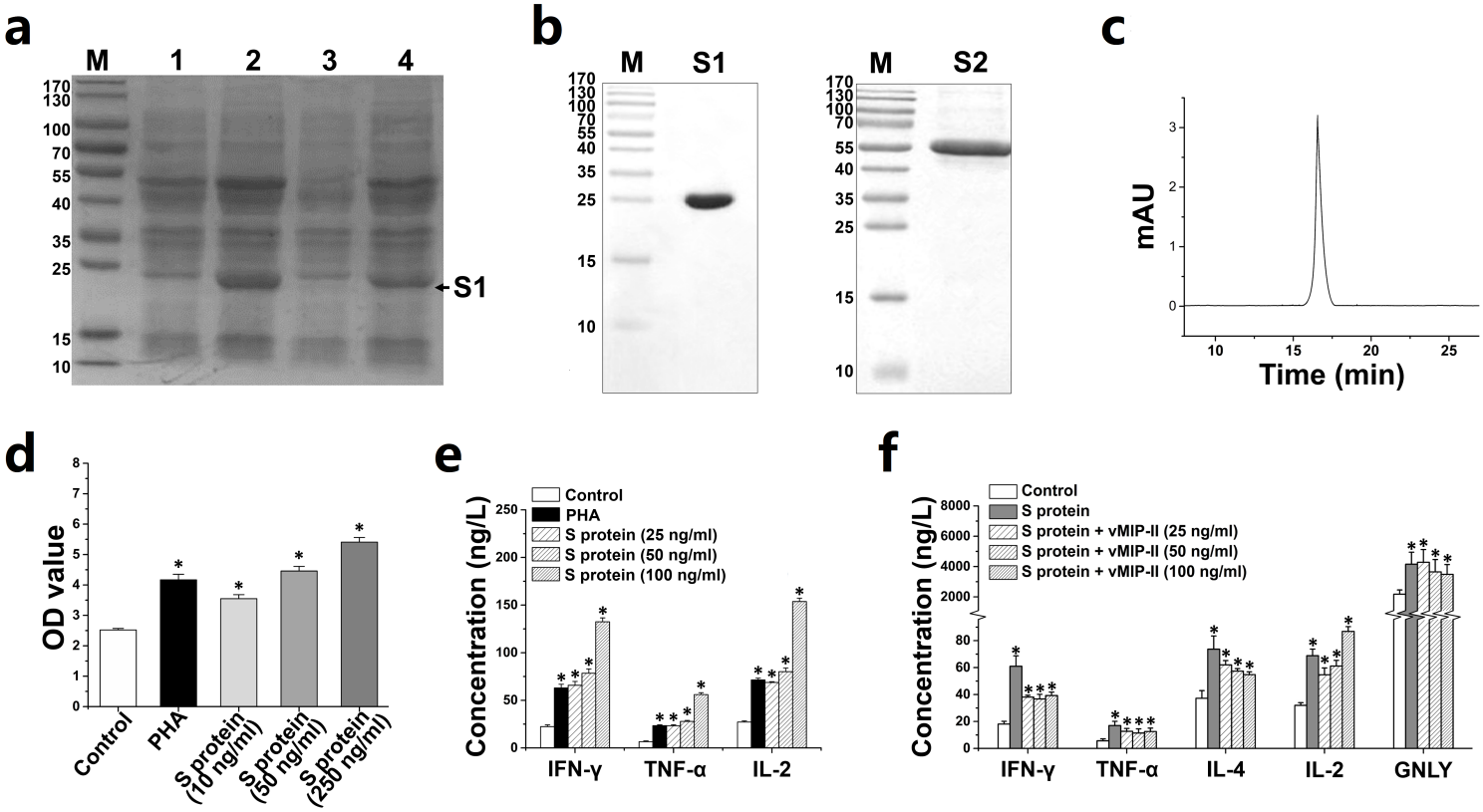

Figure 1

Clone, expression and antigenic activity of COVID-19 S protein a SDS-PAGE electrophoresis of S1 and S2 cloned. S1 and S2 gene of SARS-CoV2 were amplified and recombined into pQE-TriSystem plasmid with His tag to obtain pSARS-CoV2-S1 and pSARS-CoV2-S2, which were transfected into E.coli M15 respectively. The E.coli expressing S1 protein of about 25 kDa was induced by 1mM IPTGat 37 ℃ for 4 hours at 250 rpm. b Electrophoretic identification of purified S1 and S2 protein. Purification>95%. c HPLC of purified S1 protein. The chromatographic conditions as follow: 20 ℃, 1 mL/min, 20 ul, wavelength: 445nm. Mobile phase A is acetonitrile: water (v/v = 9:1) and mobile phase B is ethylacetate. d Cell proliferation of PBMCs stimulated by S protein by MTT method. S protein (10, 50, 250ng/ml) and PHA (2 μg/ml) to control , * p-value □ 0.05. e Cytokine secretion of PBMCs stimulated by different doses of S protein. There was a dose-dependent relationship. * p-value □ 0.05.; ** p-value □ 0.01, compared with control. f vMIP-II affected the cytokine secretion stimulated by S protein. Compared with the S protein group, * p-value □ 0.05, ** p-value □ 0.01.

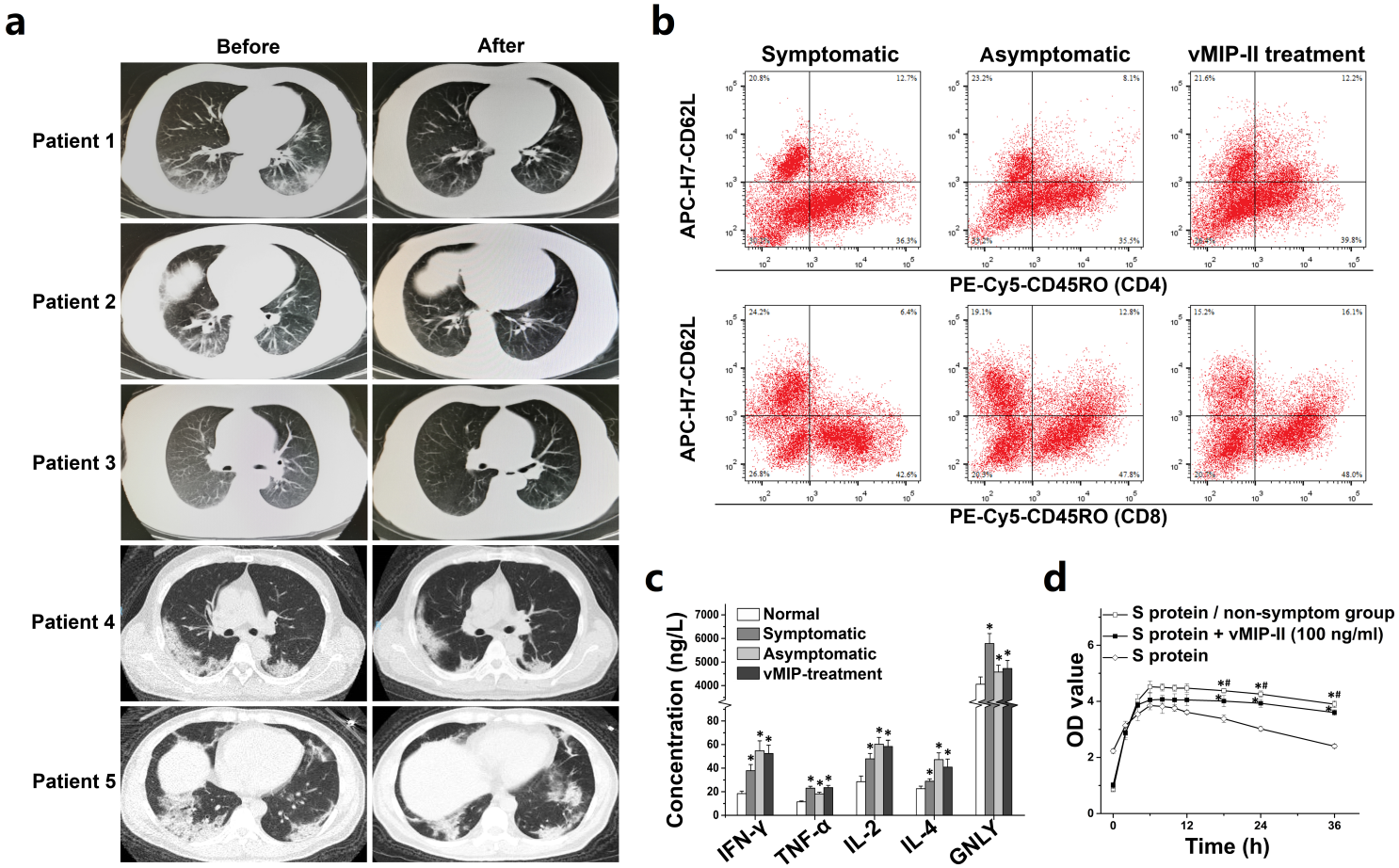

Figure 2

Clinical study of novel coronavirus pneumonia treated by vMIP-II. a Reduction of lesions of lung CT treated by vMIP-II. Five common patients with SARS-CoV-2 virus were scanned by lung CT before and one week after vMIP-II treatment. The ground glass lesions and white areas of the lungs were significantly alleviated after one-week treatment. b Analysis of T cell subgroups in PBMCs of convalescent patients after one week of being the virus negative. c Cytokine level of different groups of PBMCs stimulated by S protein in convalescent patients after one week of being negative. Different groups of separated PBMCs

was added with S protein (100 ng/ml S1+ S2, w/w = 2:1) and detected by cytokine kits, * p-value 0.05. d Proliferation of PMBCs stimulated by S protein in convalescent groups after one week of being negative. Compared with the common symptomatic group, vMIP-II group and non-symptomatic group* p-value 0.05. (n = 5).

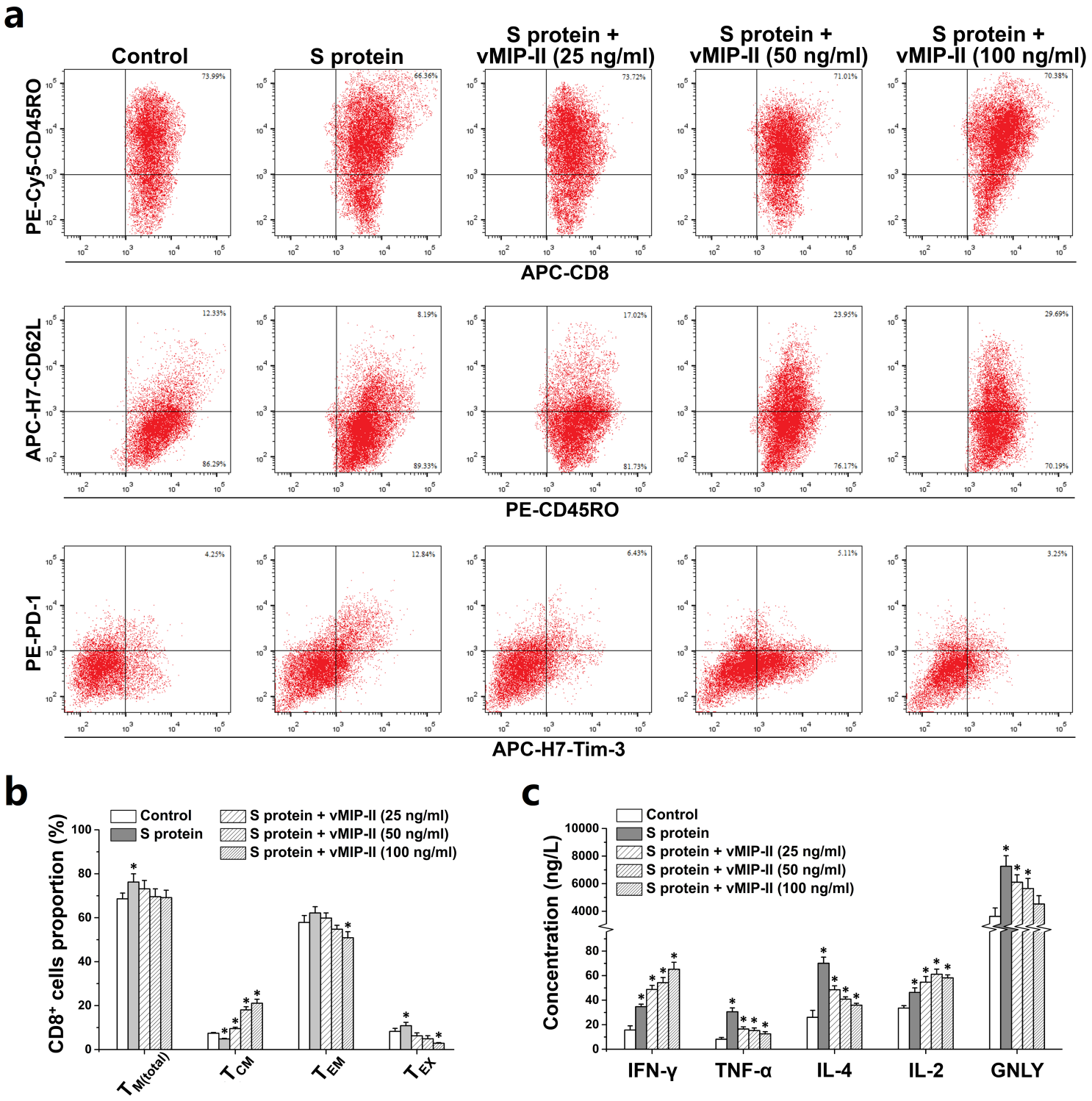

Figure 3

The effect of vMIP-II on the differentiation of effector CD8+T stimulated by S protein. a Flow cytometry detection of memory CD8+ T cells. Different subgroups of memory CD8+ T cells were distinguished by

CD45RA and CD62L. The third line was the detection of inhibitory molecules on the surface of CD8+ T cells. The depleted CD8+ T cells (TEX) were distinguished by the highly expressed inhibitory molecules PD-1 and Tim-3. b Proportion and distribution of CD8+ T cell subgroups in different vMIP-II to S protein. Compared with control group, * p-value 0.05. (n = 3). c The effects of vMIP-II on the level of cytokines secretion of CD8+T cells induced by S protein. Compared with the S protein group, * p-value < 0.05

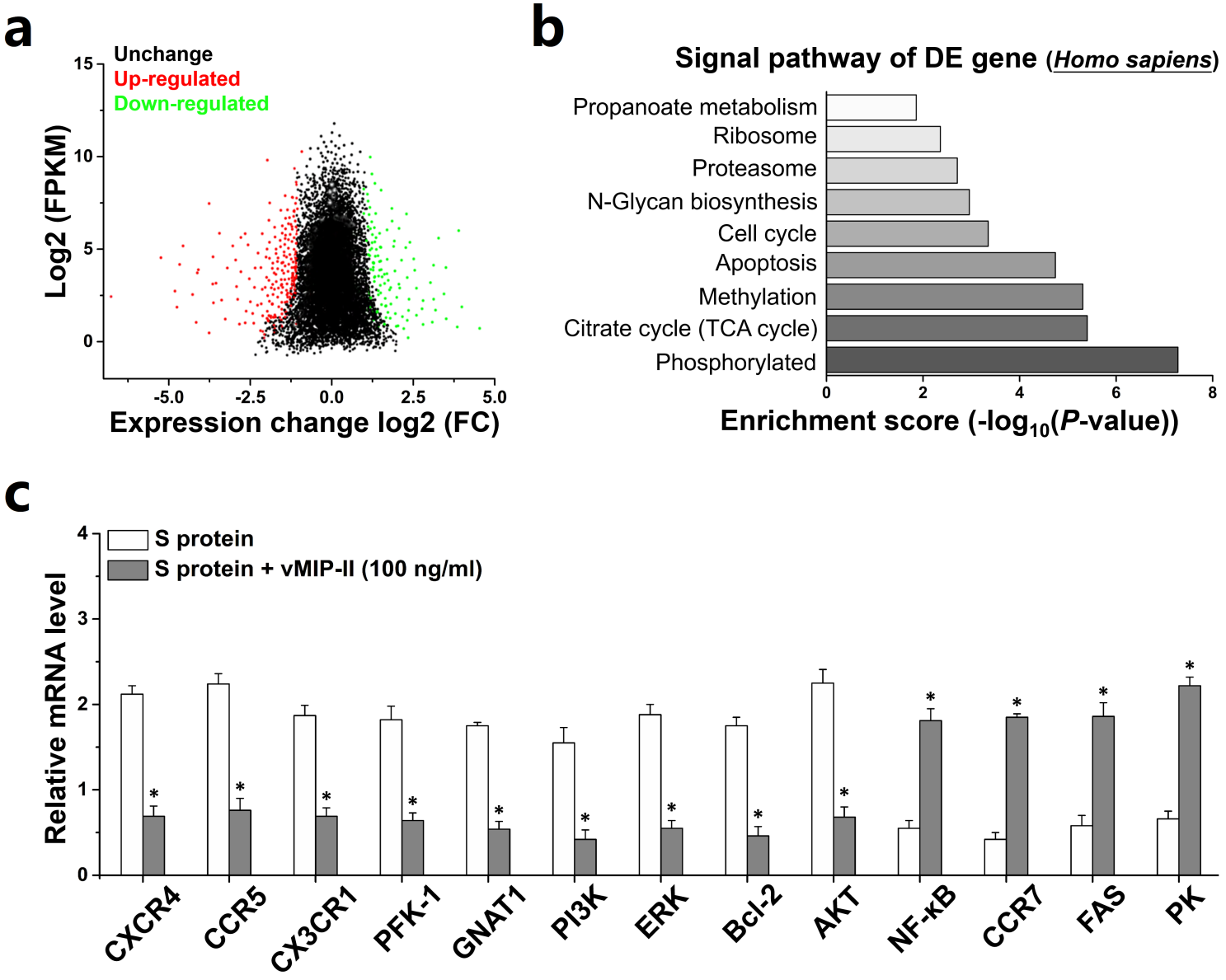

Figure 4

Difference of gene expression in CD8+T cells with treated by vMIP-II. a MA map of differentially expressed genes. Gene differential expression analysis on effector CD8+T cells sample of vMIP- treatment group and S protein group was performed by DESeq. b Analysis of KEGG pathway of differentially expressed genes. c qRT-PCR verification of differentially expressed genes. Compared with the S protein group, * p-value 0.01

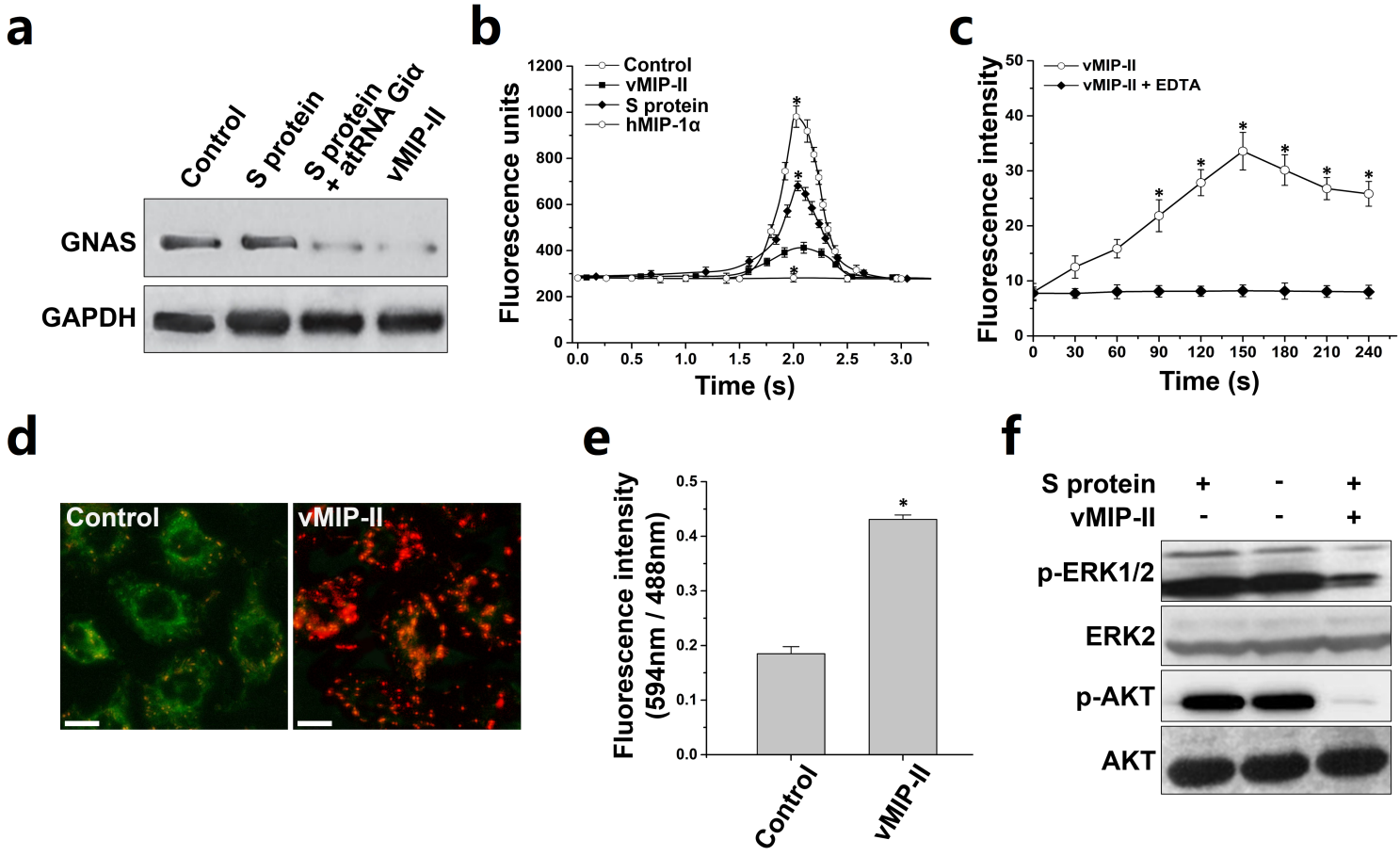

Figure 5

The effects of vMIP-Ⅱ on the signal pathway of effector CD8+T cells. a Western blot detection of G protein expression in effector CD8+T cells decreased by vMIP-Ⅱ. The decrease of G protein induced by vMIP-II was more obvious in the presence of Giα antisense oligodeoxynucleotides. b vMIP- Ⅱ significantly inhibited the rapid calcium inflow in cells, compared with control, S protein and hMIP-1Ⅱ group p-value < 0.01. c The intracellular chelate calcium increased by the treatment with vMIP-Ⅱ, compared with the control group, p-value < 0.01. d,e vMIP-Ⅱ increased the mitochondrial membrane potential of CD8+T cells, The left is control group, the right is vMIP-II treatment group. compared with the control group, intensity of fluorescent color, p-value < 0.01. f The effect of vMIP-Ⅱ on phosphorylation of MAPK/ERK and Akt. Stimulated by the S protein, CD8+T cells were co-incubated with or without vMIP-II. The results showed the level of phosphorylation evidently decreased in the presence of vMIP-II.

Supplementary Files

This is a list of supplementary files associated with this preprint. Click to download.

- SupplementaryInformation.docx